

# The metallicity distribution of F/G dwarfs derived from BATC survey data

Cui-hua Du<sup>1,2</sup>, Xu Zhou<sup>1</sup>, Jun Ma<sup>1</sup>, Jian-rong Shi<sup>1</sup>, Alfred Bing-Chih Chen<sup>3</sup>,  
Zhao-ji Jiang<sup>1</sup>, Jian-sheng Chen<sup>1</sup>

Received \_\_\_\_\_; accepted \_\_\_\_\_

---

<sup>1</sup>National Astronomical Observatories, Chinese Academy of Sciences, Beijing, 100012, P. R. China;  
dch@vega.bac.pku.edu.cn

<sup>2</sup>College of Physical Sciences, Graduate School of the Chinese Academy of Sciences, Beijing, 100012, P.  
R. China

<sup>3</sup>Department of Physics, National Cheng Kung University, Taiwan 70148, Taiwan

## ABSTRACT

Based on synthetic flux spectra calculated from theoretical atmospheric models, a calibration of temperature and metallicity for the dwarfs observed in the Beijing-Arizona-Taiwan-Connecticut (BATC) multicolor photometric system is presented in this paper. According to this calibration, stellar effective temperatures can be obtained from some temperature-sensitive color indices. The sample stars have colors and magnitudes in the ranges  $0.1 < d - i < 0.9$  and  $14.0 < i < 20.5$ . The photometric metallicities for these sample stars can be derived by fitting SEDs. We determine the average stellar metallicity as a function of distance from the Galactic plane. The metallicity gradient is found to be  $d[\text{Fe}/\text{H}]/dz = -0.37 \pm 0.1$  dex/kpc for  $z < 4$  kpc and  $d[\text{Fe}/\text{H}]/dz = -0.06 \pm 0.09$  dex/kpc between 5 and 15 kpc. These results can be explained in terms of different contributions in density distribution for Galactic models ‘thin disk’, ‘thick disk’ and ‘halo’ components. However, for the gradient in  $z > 5$  kpc, it could not be interpreted according to the different contributions from the three components because of the large uncertainty. So it is possible that there is little or no gradient for  $z > 5$  kpc. The overall distribution shows a metallicity gradient  $d[\text{Fe}/\text{H}]/dz = -0.17 \pm 0.04$  dex/kpc for  $z < 15$  kpc.

*Subject headings:* Galaxy: abundances—Galaxy: disk—Galaxy: halo—Galaxy: structure—Galaxy: formation.

## 1. INTRODUCTION

The Galaxy is unique in offering the possibility of determining directly the three-dimensional distributions of luminous mass and chemical abundances. Combination of these results allows a detailed investigation of the dominant physical processes that occurred during the formation and early evolution of the Galaxy (Gilmore & Wyse 1985). Over the past decade considerable efforts have been undertaken to gain information about the structure and formation of the Galaxy.

Of crucial importance in the structure and formation of the Galaxy is the existence of a thick disk component. Ever since it was revealed that the Galactic disk contains two distinct stellar populations, the origin and nature have been discussed by a number of investigators. The thick disk population was evident in the data of Hartkopf & Yoss (1982) and clearly explained by Gilmore & Reid (1983). While subsequent investigations have determined the overall kinematic and chemical properties of the thick disk rather well (Gilmore & Wyse 1985; Sandage & Fouts 1987; Majewski 1992; Reid et al. 1993; Robin et al. 1996), the relation of the thick disk to the halo population and to the thin disk as well as its evolutionary history are still poorly known (Gilmore 1989). Also, the formation of the thick disk component is also an open question. A number of models for the formation of the thick disk have been put forward since the confirmation of its existence. Sandage (1990) proposed that the thick disk was formed by dissipative pressure-supported collapse in the early history of the Galaxy, producing a kinematic and chemical gradient as the gas was settling into the galactic plane. Other scenarios of the thick disk formation, including that in which the thick disk is the result of an accretion induced heating of the thin disk, were discussed by Majewski (1993). In order to study the formation process of the thick disk in more detail, additional information such as the metallicity gradient is also needed. If the detailed information becomes available, it is possible to provide clues not only for the formation history of the thick disk, but also for the Galaxy as a whole.

Numerous surveys along the Galactic plane have been used to investigate the existence and size of the galactic radial abundance gradient in the disk. A wide variety of objects have been used to determine this gradient, from radio and optical observation of HII regions, disk stars (Neese & Yoss 1988), planetary nebulae (Shaver et al. 1983; Pasquali & Perinotto 1993; Henry & Worthey 1999; Hou et al. 2000; Maciel et al. 2003) and open clusters (Friel 1995; Chen et al. 2003). The existence of a radial gradient in the Galaxy is now well established. An average gradient of about  $-0.06 \text{ dex kpc}^{-1}$  is observed in the Galactic disk for most of the elements (Chen et al, 2003). On the other hand, there is considerable disagreement about whether there is a vertical metallicity gradient among field and/or open cluster stars of the Galactic disk. Its extent and reasons are not well understood either, yet potentially it must be a powerful clue to the Galactic formation. The amplitude of any vertical gradient of stellar properties allows one to place constraints on the existence of discrete stellar subpopulation and/or distinct components of the Galaxy (Sandage 1981).

The BATC multicolor photometric survey accumulated a large data base which is very useful for studying the structure and formation of the main components of the Galaxy. Du et al. (2003) provided some information on the density distribution of the main components of the Galaxy, which can present constraints on the parameters of models of the Galactic structure. Here, we shall use F and G dwarfs from the BATC survey data to provide the metal-abundance information. The main sequence lifetime of F and G type stars is longer than the age of the Galaxy, and hence the chemical abundance distribution function of such stars provides an integrated record of the chemical-enrichment history (Chen et al. 2000). Many general trends have been discovered during the past decades. With the new improved observation and improved knowledge regarding galaxy formation, it becomes possible to further discuss the metallicity gradient in the Galaxy.

In this paper, we attempt to study the metallicity gradient of the Milky Way galaxy using the BATC photometric survey data. The outlines of this paper is as follows. The BATC photometric system and data reduction are introduced briefly in Sect. 2. In Sect. 3 we describe the theoretical model atmosphere spectra and synthetic photometry. In Sect. 4, we present the BATC data used in this analysis. The vertical metallicity gradient is discussed in Sect. 5. In Sect. 6, an estimation for metallicity gradient using a three-component model is made and the result is compared with the observed metallicity gradient. Finally, in Sect. 7 we summarize our main conclusions in this study.

## 2. BATC PHOTOMETRIC SYSTEM AND DATA REDUCTION

The BATC program uses the 60/90 cm f/3 Schmidt telescope at the Xinglong Station of the National Astronomical Observatories (NAOC), with a  $2048 \times 2048$  Ford CCD mounted at its focal plane. The field of view of the CCD is  $58' \times 58'$ , with a pixel scale of  $1''.7$ . There are 15 intermediate-band filters in the BATC filter system, which covers an optical wavelength range from 3000 to 10000 Å. Fig. 1 shows the filters transmissions. The well-known advantage of using these filters is that intermediate bandwidths can ignore color terms for atmospheric extinction correction, as opposed to such a necessity for broad band filters. The BATC magnitudes adopt the monochromatic AB magnitudes as defined by Oke & Gunn (1983). The standard stars HD19445, HD84937, BD+262606 and BD+174708 (Oke & Gunn 1983) are observed for flux calibration in the BATC survey. The detailed description of the BATC photometric system and flux calibration of the standard stars can be found in Fan et al. (1996) and Zhou et al. (2001, 2003).

The BATC survey images were reduced through standard procedures, including bias subtraction, flat-fielding correction and flux calibrations (Fan et al. 1996; Zhou et al. 2001; Zhou et al. 2003). After the basic corrections described above, the multiple field images observed of each filter were combined by integer pixel shifting, respectively. When combining the images, the cosmic rays and bad pixels were corrected by comparison of multiple images. The HST Guide star catalog (GSC) (Jenkner et al. 1990) was then

used for coordinate determination. The final RMS error in positions of GSC stars is about 0.5 arcsec. The magnitudes of the point sources in the BATC fields are measured by the photometric method of point spread function (PSF) fitting. Our PSF magnitudes were obtained through an automatic data reduction program PIPELINE 2, which was developed based on Stetson’s DAOPHOT procedures (Stetson 1987). Finally, at the completion of photometry, the spectral energy distribution (SEDs) of all measurable objects are obtained.

### 3. THEORETICAL MODEL AND CALIBRATION FOR TEMPERATURE AND METALLICITY

#### 3.1. Theoretical stellar library and synthetic photometry

A homogeneous and complete stellar library can match any ambitious goals imposed on a standard library. Lejeune et al. (1997) presented a hybrid library of synthetic stellar spectra. The library covers a wide range of stellar parameters:  $T_{\text{eff}}=50,000$  K to 2,000 K in intervals of 250 K,  $\log g=-1.02$  to 5.50 in main increments of 0.5, and  $[M/H]=-5.0$  to  $+1.0$ . For each model in the library, a flux spectrum is given for the same set of 1221 wavelength points covering the range 9.1 to 160,000 nm, with a mean resolution of 20Å in the visible. The spectra are thus in a format which has proved to be adequate for synthetic photometry of wide band and intermediate band systems.

Based on the theoretical library, we calculate synthetic colors of the BATC system. Here, we synthesize colors for simulated stellar spectra with  $T_{\text{eff}}$  and  $\log g$  characteristic of F/G dwarfs ( $\log g=4.0, 4.5$  for dwarfs) and 19 values of metallicity ( $[M/H]=-5.0, -4.5, -4.0, -3.5, -3.0, -2.5, -2.0, -1.5, -1.0, -0.5, -0.3, -0.2, -0.1, 0.0, +0.1, +0.2, +0.3, +0.5$  and  $+1.0$ ), where  $[M/H]$  denotes metallicity relative to hydrogen. The synthetic  $i$ th BATC filter magnitude can be calculated with

$$m = -2.5 \log \frac{\int F_{\lambda} \phi_i(\lambda) d\lambda}{\int \phi_i(\lambda) d\lambda} - 48.60, \quad (1)$$

where  $F_{\lambda}$  is the flux per unit wavelength,  $\phi_i$  is the transmission curve of the  $i$ th filter of the BATC filter system (Fig. 1). In Fig. 2, as an example, we present the two-color diagram based on  $c, i, p$  filters. From this figure, we can clearly see how the color indices vary as a function of temperature and metallicity. In this two-color diagram, the gravity  $\log g=4.5$  corresponds roughly to dwarfs. Four metallicities:  $[M/H]=-5.0, -1.5, 0.0$  and  $+1.0$  are arbitrarily selected and the temperature range is  $5000 \text{ K} \leq T_{\text{eff}} \leq 8000 \text{ K}$ . For clarity, the grid points are connected with lines, illustrating isothermal and iso-metallicity lines. Similar grids, of course, exist as well for other two-color diagrams with different gravities and metallicities in the library.

The bluer colors are sensitive to metallicity down to the lowest observed metallicities because most of

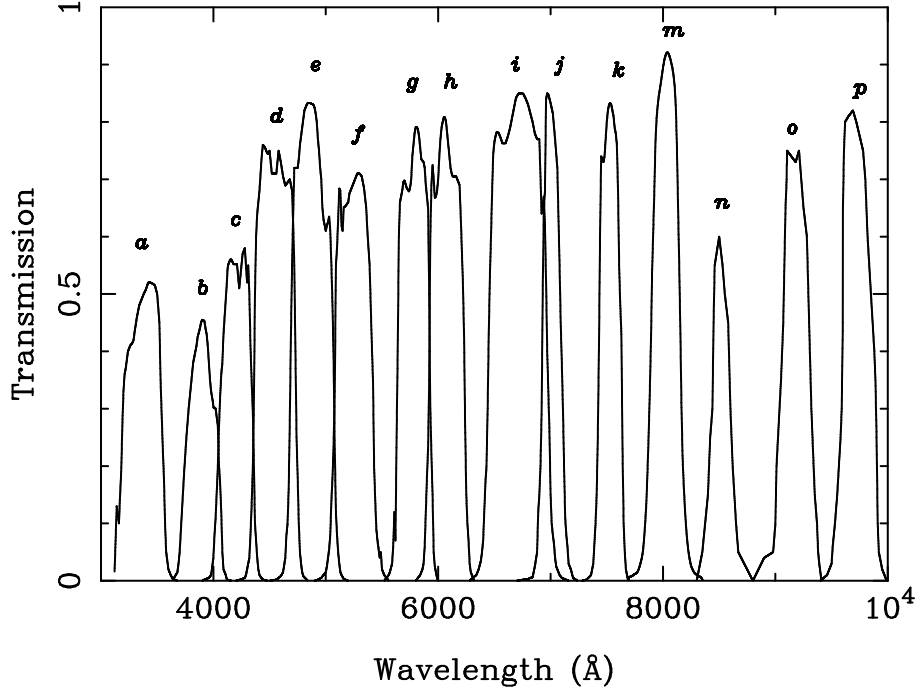


Fig. 1.— The transmission curves for the BATC multicolor filters.

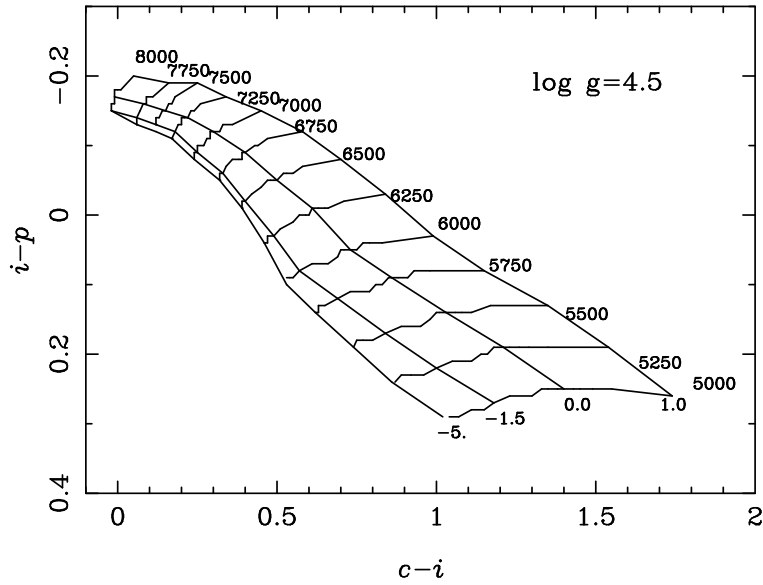


Fig. 2.— The  $i-p$  versus  $c-i$  diagram. A grid of constant- $\log g$  models with the metallicities:  $[M/H] = -5.0, -1.5, 0.0$  and  $+1.0$ ; and with  $T_{\text{eff}} \geq 5000$  K are presented in the two-color diagram. The grid points are connected with straight lines, illustrating isotherm and iso-metallicity lines.

the line-blanketing from heavy elements occurs in the shorter wavelength regions. In contrast, the redder colors are primarily sensitive to temperature index. The BATC  $a$ ,  $b$  bands contain the Balmer jump, a stellar spectral feature which is sensitive to surface gravity. Since our sample includes only F/G dwarfs, it conveys little gravity information. Therefore, we shall focus on effective temperature and metallicity in the following sections. It should be mentioned that, although the metallicity or temperature derived from synthetic photometry is not very accurate for a single star, perhaps which can be distorted by a poor point, it is meaningful by studying sample stars.

### 3.2. Temperature and color index

The stellar effective temperature can be derived by comparing observed SEDs with theoretical ones. In general, a sensitive color index can represent this physical quantity, such as  $b - y$  in the  $ubvy$  system (Ardeberg et al. 1983). We would like to find such color indices which are sensitive to the effective temperature in the BATC filter system. Our study shows that color indices  $d - n$ ,  $d - o$ ,  $e - o$  and  $e - p$  are very sensitive to temperature but are relatively insensitive to  $\log g$  and  $[M/H]$ . In Fig. 3, the relationships between  $\log (T_{\text{eff}})$  and color index are shown, and the correlation between  $\log (T_{\text{eff}})$  and color index is nearly linear. The symbol dots represent a grid of theoretical models for different metallicity F/G dwarfs. As shown in Fig. 3, a simple polynomial can describe the relationship between  $\log (T_{\text{eff}})$  and color indices. A quadratic polynomial is as follows:

$$\log (T_{\text{eff}}) = A_0 + A_1(CI) + A_2(CI)^2, \quad (2)$$

where  $CI$  is the color index. The coefficients of equation (2) for different color indices are listed in Table 1. The final photometric effective temperature can be derived by making the mean value among the four temperatures from the different color indices. Chen et al. (2000) used the most temperature-sensitive color index in their study to derive the effective temperature. Our results show that our fitting on  $d - o$  is very close to the red region of their fitting on NGC 288 stars.

Table 1: Coefficients of the color index and effective temperature relation

Color index	$A_0$	$A_1$	$A_2$	$\chi^2$
$d - n$	3.8474	-0.1620	-0.0031	0.011
$d - o$	3.8471	-0.1663	0.0158	0.011
$e - o$	3.8423	-0.1884	0.0270	0.013
$e - p$	3.8408	-0.1873	0.0327	0.013

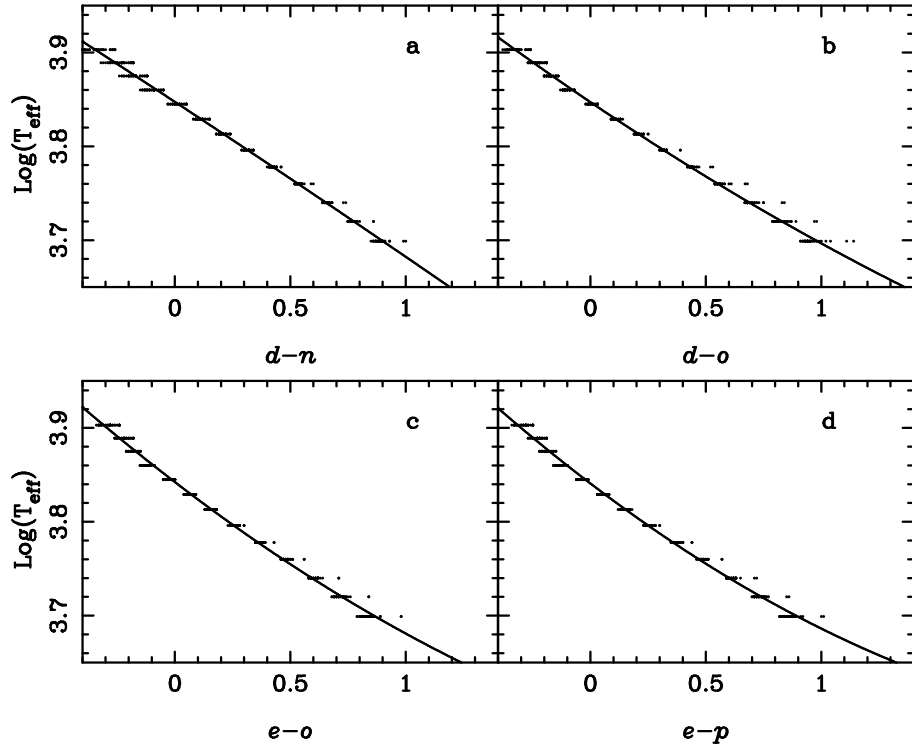


Fig. 3.— The relationship between  $\log (T_{\text{eff}})$  and the color indices of bandpasses relatively insensitive to  $\log g$  in our data for (a)  $d-n$ , (b)  $d-o$ , (c)  $e-o$ , (d)  $e-p$ . The symbol dots represent a grid of theoretical models for different metallicity dwarfs.



### 3.3. Metallicity and abundance

Photometric indices were often used to give the stellar metallicity. For example, Wallerstein (1962) derived the [Fe/H] calibration using the  $\delta(U - B)$  excess of the Johnson  $UBV$  photometric system. For the *uvby* system, Crawford (1975a), Nissen (1981) and Olsen (1988) used the photometric differentials  $\delta m_1$  and  $\delta c_1$  to derive the [Fe/H] calibration. Following that, Schuster & Nissen (1989) made direct use of the photometric indices  $m_1$  and  $c_1$  to derive [Fe/H] calibrations for F and G dwarfs.

For the BATC multicolor photometric system, there are 15 intermediate band filters covering an optical wavelength range from 3000 to 10000 Å. So the SEDs of 15 filters for every observed object are equivalent to a low resolution spectra. Using the equation (2), the effective temperature of a given star can be derived in advance from the available photometry. Thus, given a photometrically determined effective temperature, we can use the SED simulation to derive the stellar metallicity. The standard  $\chi^2$  minimization, i.e., computing and minimizing the deviations between the photometric SED of a star and the template SEDs obtained with the same photometric system, is used in the fitting process. The minimum  $\chi^2_{min}$  indicates the best fit to the observed SED by the set of template spectra:

$$\chi^2 = \sum_{l=1}^{N_{filt}=15} \left[ \frac{m_{obs,l} - m_{temp,l} - b}{\sigma_l} \right]^2, \quad (3)$$

where  $m_{obs,l}$ ,  $m_{temp,l}$  and  $\sigma_l$  are the observed magnitude, template magnitude and their uncertainty in filter  $l$ , respectively, and  $N_{filt}$  is the total number of filters in the photometry, while  $b$  is the mean magnitude difference between observed magnitude and template magnitude. The uncertainties of metallicity obtained from comparing SEDs between photometry and theoretical models are due to the observational error and the finite grid of the models (Chen et al. 2000). For the metal-poor stars ([Fe/H] < -1.0), the metallicity uncertainty is about 0.5 dex, and 0.2 dex for the stars [Fe/H] > -0.5.

## 4. PHOTOMETRIC DATA

### 4.1. Object classification and photometric parallaxes

In this study, we use two fields at intermediate latitudes;  
— BATC T329 field with central coordinates  $\alpha = 09^h53^m13^s30$  and  $\delta = 47^\circ49'00''0$  (J2000) (Galactic coordinates:  $l = 169.95^\circ, b = 49.80^\circ$ ). It is complete to 20.5 mag with an error of less than 0<sup>m</sup>.1 in the BATC  $i$  band. Each object is classified according to their SED information constructed from the 15-color photometric catalog. The observed colors of each object are compared with a color library of known objects with the same photometric system. Firstly, we use spectral templates of galaxies and stars to discriminate the stars from galaxies. The profile of objects classified as stars does not deviate significantly from that of stellar templates. The input library for stellar spectra is the Pickles (1998) catalog. Details about the

classification of galaxies are given in Xia et al. (2002) and stars given in Du et al. (2003). The limiting magnitude is not so deep as to be strongly contaminated by a lot of galaxies, and the possibility of galaxy contamination is estimated to be less than 3%.

— BATC TA01 field with central coordinates  $\alpha = 01^h 12^m 06^s 00$  and  $\delta = -00^\circ 02' 00''$  (J2000) (Galactic coordinates:  $l = 134.16^\circ, b = -62.45^\circ$ ). It is complete to  $20^m 0$  in the BATC  $i$  band. It should be noted that the stars-galaxies separation for the BATC TA01 field is different from the BATC T329 field. Because the BATC TA01 field has been observed by the Sloan Digital Space Survey (*SDSS*) and each object type (stars-galaxies-QSO) has been given, we can make direct use of those stars to obtain star types according to the stellar spectra library.

According to the results of object classification, we pick out the F/G dwarfs from the two fields. Details about the classification of stars can be found in Du et al. (2003). In total, there are 383 F/G dwarfs, and the photometric parallaxes can be obtained according to the stellar types. In Fig. 4, we give the actual  $z$  distance distribution for two fields. It is clear that most of stars are in  $z \sim 1 - 2$  kpc for the two fields. A variety of errors affect the determination of stellar distances. The first source of errors is from photometric uncertainty less than 0.1 mag in the BATC  $i$  band; the second from the misclassification, which should be small due to the multicolor photometry. For luminosity class V, types F/G, the absolute magnitude uncertainty is about 0.3 mag. In addition, there may exist an error from the contamination of binary stars in our sample. **We neglect the effect of binary contamination on distance derivation due to the unknown but small influence from mass distribution in binary components (Kroupa et al. 1993; Ojha et al. 1996).** The two fields lie in intermediate latitudes and the influence of interstellar extinction in the distance calculation can be neglected.

#### 4.2. Classification comparison and stellar population

The stellar classifications are compared between stellar spectra library from Pickles (1998) and theoretical spectra library from Lejeune (1997). In our previous paper (Du et al. 2003), we derived the stellar type according to Pickles stellar spectra library (Pickles 1998). To obtain more information about metallicity, we here use theoretical spectra library from Lejeune (1997) to derive the stellar parameters such as temperature and metallicity. In order to check the agreement between the Pickles library and Lejeune library, we present a comparison.

As an example, Table 2 lists the comparison results between Pickles spectra and Lejeune spectra for six stars in our sample. The first column is the stellar type derived from Pickles library. According to the theoretical library from Lejeune (1997), the effective temperature  $T_{\text{eff}}$  is determined by using equation (2), and it is listed in the second column. The gravity  $\log g$  and metallicities ( $[\text{Fe}/\text{H}]$ ) are also derived by fitting SEDs according to the theoretical library from Lejeune (1997). They are listed in the following two

columns. The apparent visual magnitude  $V$  and photometric distances are listed in the last two columns. **As listed in Table 2, our classification results from Pickles library (1998) are in excellent agreement with theoretical library from Lejeune (1997).** The metallicities ( $[\text{Fe}/\text{H}]$ ) for these stars can only provide an estimate of individual stellar abundances, but we have the advantage of being able to use many stars to obtain mean metallicity at different distances from the plane.

Table 2: Classification comparisons between stellar synthetic spectra from Lejeune (1997) and stellar library from Pickles (1998)

type	$T_{\text{eff}}$	$[\text{Fe}/\text{H}]$	$\log g$	$V$	$r$ (kpc)
G8V	5110	-2.0	4.5	18.2	2.9
G5V	5330	-1.0	4.5	17.2	2.4
G3V	5470	-0.5	4.0	16.1	1.8
G0V	5717	-1.0	4.5	16.5	2.4
F7V	6047	-0.3	4.5	14.6	1.5
F5V	6273	-3.5	4.0	17.0	4.0

Standard star-count models indicate that the color-magnitude range could be used to separate roughly different populations of the Galaxy (Chen et al. 2001, Du et al. 2003). The present sample stars have colors and magnitudes in the ranges  $0.1 < d - i < 0.9$  and  $14.0 < i < 20.5$ . According to star-count models, the present sample should contain predominantly thick disk stars in the color-magnitude range, with some contributions from the thin disk and halo near the edge of the sample selection. As shown in Fig. 5, there are no stars redder than  $(d - i) \sim 0.9$ . For the T329 field, the stars distribution is smooth, while there is a sharp increase at  $(d - i) \sim 0.6$  for the TA01 field. The peak values for the two fields, however, lie in  $(d - i) \sim 0.6$ . We use the Galaxy models to predict the relative frequency of dwarfs belonging to each of the three dominant components in the Galaxy. These relative frequencies obviously depend on both the local normalization of each component’s density distribution and its scale height. The density distributions can be combined with the local volume element to produce estimates of the number of stars from given components expected to be observed at a given height above the plane (Gilmore & Wyse 1985),

$$n_i(z) = \rho_{0i} \exp(-z/z_{0i}) z^2 dz, \quad (4)$$

where the subscript  $i$  refers to each component,  $\rho_0$  being the local density normalization, and  $z_0$  the scale height. The components are (i) the thin disk with local normalization 1.0 and an exponential scale height of 320 pc (Du et al. 2003); (ii) the thick disk, with local normalization 0.07 and exponential scale height of 640 pc (Du et al. 2003); and (iii) the halo, with local normalization 0.00125 and  $R^{1/4}$  density distribution

with axial ratio of 0.6, and an effective radius of 2.7 kpc (Du et al. 2003). The resultant curves for various components of the Galaxy are shown in Fig. 6. The solid line, dotted-dashed line and dotted line represent the contribution of the halo, thick disk and thin disk, respectively. The various curves are normalized independently of each other. In Table 3, we show the logarithmic numbers as functions of height. The number of stars in the thin disk, thick disk, and halo are represented by  $n_0$ ,  $n_1$  and  $n_2$  respectively. The curves in Fig. 6, when combined with local normalization, mean that the thin disk will contribute up to  $z$  heights of about 1 kpc, while the thick disk will dominate from 1 kpc to 4 kpc.

Table 3: The number of stars versus the distance  $z$  for three components of the Galaxy

$z$ (kpc)	$\log (n_0)$	$\log (n_1)$	$\log (n_2)$
0.05	4.03	2.91	1.19
0.69	5.44	4.76	3.36
1.34	5.13	4.89	3.81
1.98	4.60	4.79	4.03
2.63	3.97	4.60	4.14
3.27	3.28	4.35	4.20
3.92	2.57	4.07	4.23
4.57	1.82	3.77	4.24
5.21	1.06	3.44	4.24
5.86	0.29	3.11	4.23

## 5. THE VERTICAL METALLICITY GRADIENT TOWARDS HIGH LATITUDE FIELDS

It is well known that the chemical abundance of a stellar population contains much information about the population’s early evolution, while detailed information about the vertical metallicity gradient can provide an important clue about the formation scenario of stellar populations. The metallicity distribution of stars in the Galaxy has been the subject of several spectroscopic and photometric surveys (Yoss et al. 1979; Hartkopf et al. 1982; Gilmore et al. 1985; Ratnatunga et al. 1989; Friel 1988).

The existence of a vertical metallicity gradient among field and open cluster stars of the Galactic disk is controversial. For example, using DDO photometry of the late-type giants in the direction of both galactic poles, several authors found a vertical gradient ranging from approximately  $-0.2$  to  $-0.4$  dex  $\text{kpc}^{-1}$  (see Hartkopf & Yoss 1982; Yoss et al. 1987; Norris & Green 1989). Other independent studies have also shown evidence for a significant vertical gradient: Buser & Rong (1995b), using the photographic RGU data

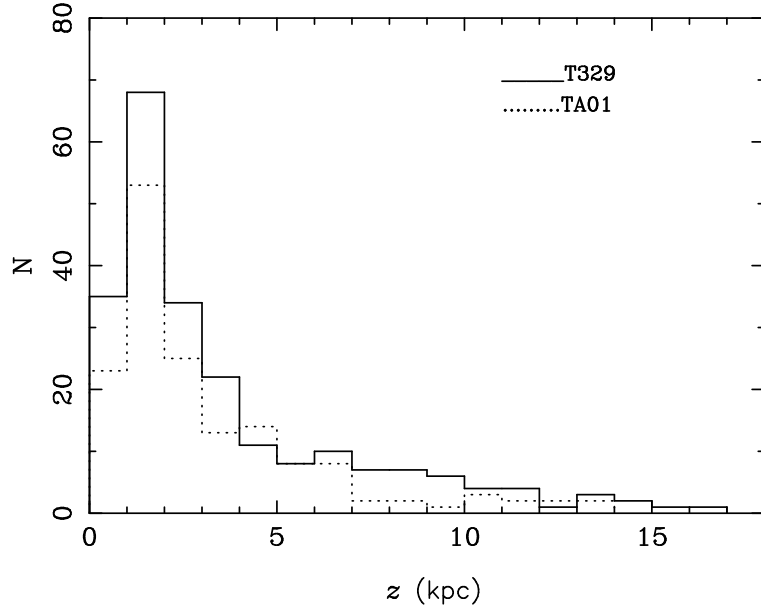


Fig. 4.— Distribution of  $z$  distance in two fields. The solid line represents the T329 field and the dotted line represents the TA01 field.

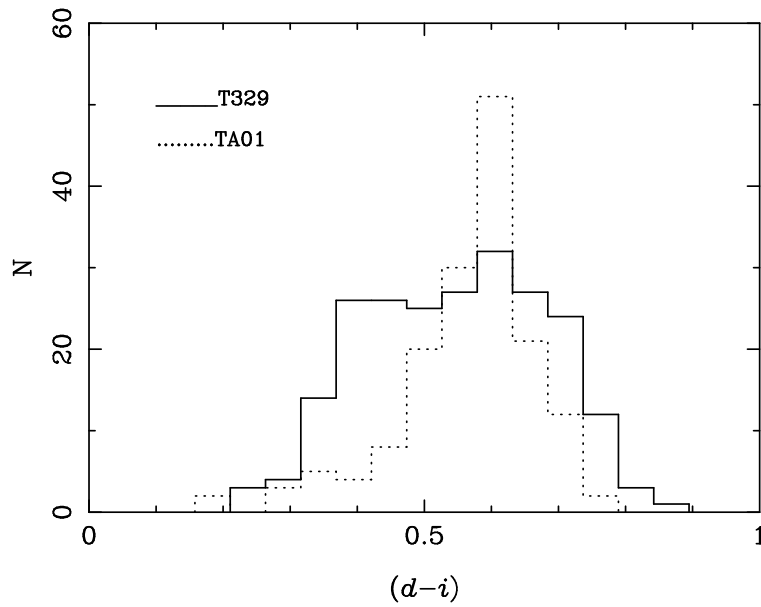


Fig. 5.— Distribution of  $(d-i)$  in two fields. The solid line represents the T329 field and the dotted line represents the TA01 field.

to study the metallicity distribution of the Galactic components, found a vertical abundance gradient of  $-0.6$  dex/kpc for the old thin disk and a marginal metallicity gradient of  $-0.1$  dex/kpc for the thick disk. Robin et al. (1996) showed that the data towards the pole are in favor of a small gradient of  $-0.25$  dex  $\text{kpc}^{-1}$ , data in SA54 field (Yamagata & Yoshii 1992) give a high value of  $-0.65$ , while data from Fenkart & Esin-Yilmaz (1985) favor a small gradient of  $-0.15$  dex  $\text{kpc}^{-1}$ . However, Gilmore (1985) showed that there is little or no gradient in the three components of the Galaxy.

Recent work has used open clusters instead of field stars to determine the metallicity gradient perpendicular to the disk. Piatti et al. (1995) found a correlation between  $[\text{Fe}/\text{H}]$  and vertical position and they obtained a gradient equal to  $-0.34$  dex  $\text{kpc}^{-1}$  by binning the data in  $z$ . Carraro (1998) also derived a vertical abundance gradient of  $-0.25$  dex  $\text{kpc}^{-1}$ . Cameron (1985) used metallicities determined from  $UBV$  photometry and found no gradient perpendicular to the plane. Friel (1995) did not find a gradient from the study of open clusters either.

In this study, we want to show how the BATC survey data can limit possible metallicity gradients for the components of the Galaxy. At first, the metallicity for the sample F/G dwarfs can be derived by comparing SEDs between photometry and theoretical models. The SEDs fitting method is already described in Sect 3.3. In Fig. 7a-e, the metallicity distributions are shown as functions of apparent magnitude for sample stars. Fig. 7f gives the metallicity distribution for all stars. Here, we divide these F/G dwarfs into 5 bins:  $14.0 < i \leq 15.5$ ,  $15.5 < i \leq 16.5$ ,  $16.5 < i \leq 17.5$ ,  $17.5 < i \leq 18.5$  and  $i > 18.5$  to see how the magnitude affects the abundance distribution. From the figures (Fig. 7a-e), we can see that there is a shift from metal-rich stars to metal-poor ones with the increasing of apparent magnitude. It is particularly apparent in Fig. 8, where the mean metallicity as a function of  $z$ -distance is displayed for the combined sample. It should be noted that we use the mean metallicity to describe the metallicity distribution function. We adopt the ‘biweight’ statistic method provided by ROSTAT software (Beers et al. 1990) to estimate the stellar mean metallicity. Although computationally more complex, the ‘biweight’ estimate has proved to be superior in many respects and has also performed well for small samples. Karaali et al. (2003) showed that the mean value is also valid to describe a distribution function.

As Fig. 8 shows clearly, the mean metal abundance decreases with the increasing mean  $z$ , indicating a clear vertical metallicity gradient of the disk ( $z < 4$  kpc). The individual fields give essentially the same result, and therefore have been combined to improve the statistics. The T329 field lies in north latitude direction and TA01 field in south latitude direction. In addition, the distributions in the two fields do not differ significantly in number of stars, so we can combine them. The overall distribution shows a metallicity gradient  $d[\text{Fe}/\text{H}]/dz = -0.17 \pm 0.04$  dex/kpc, up to 15 kpc. At the same time, we find a gradient of  $-0.37 \pm 0.1$  dex/kpc for  $z < 4$  kpc, whereas it shows a weak or zero gradient between 5 and 15 kpc, i.e.,  $d[\text{Fe}/\text{H}]/dz = -0.06 \pm 0.09$  dex/kpc.

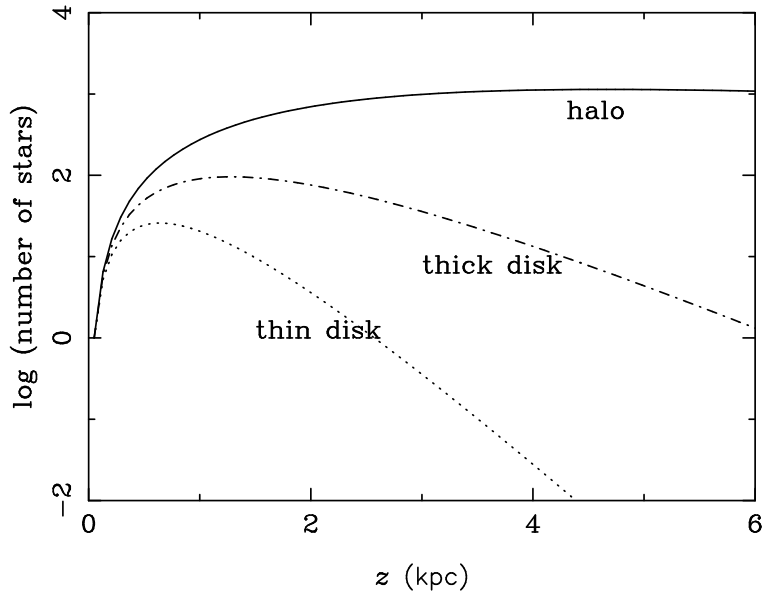


Fig. 6.— Relative number of stars within a given volume element as a function of height above the plane for various components of the Galaxy.

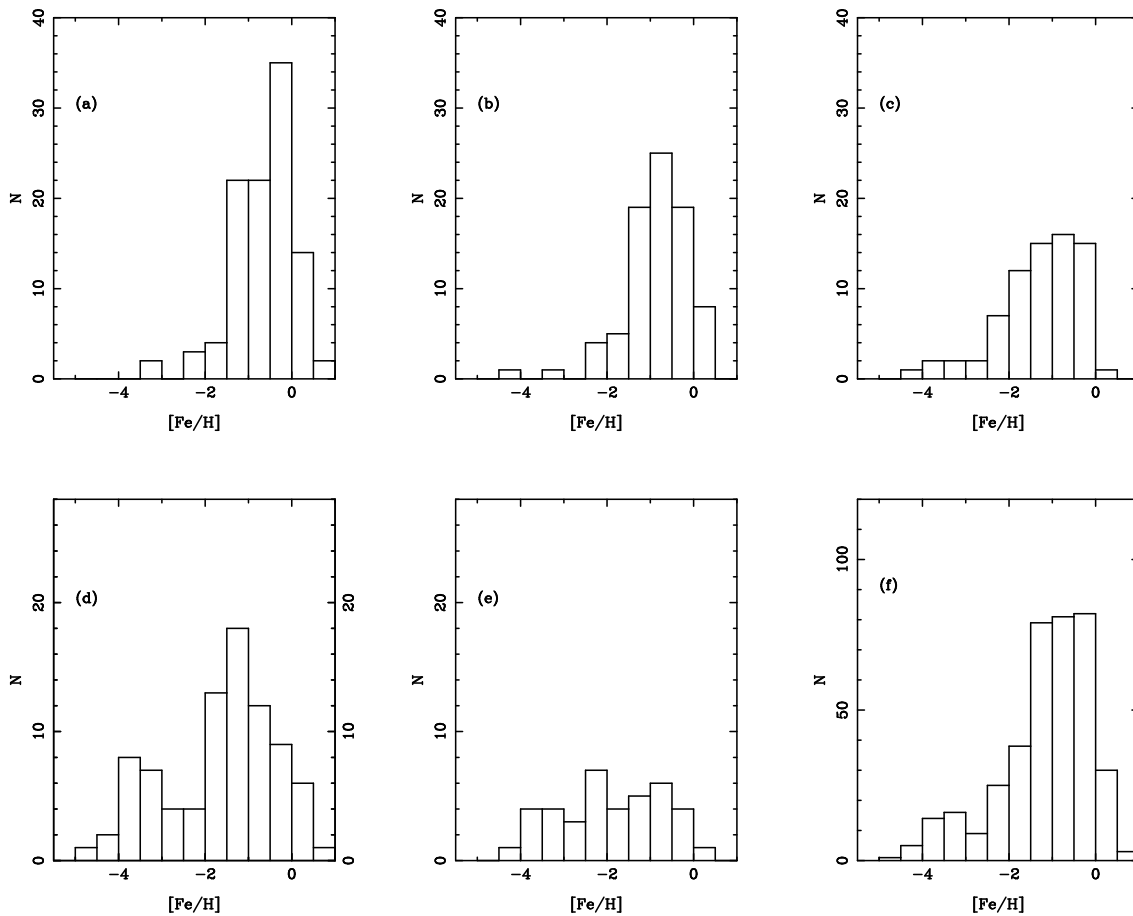


Fig. 7.— Metallicity distribution for sample stars as functions of apparent magnitude  $i$ . (a)  $14.0 < i \leq 15.5$ , (b)  $15.5 < i \leq 16.5$ , (c)  $16.5 < i \leq 17.5$ , (d)  $17.5 < i \leq 18.5$ , (e)  $i > 18.5$  and (f)  $14.0 < i \leq 20.5$ .

Based on Geneva photometry, Grenon (1977) investigated the vertical metallicity gradient for G and K giants and estimated a value of  $-0.35$  dex/kpc for  $z$  between 0 and 700 pc. Yoss et al. (1987) obtained G5-K6 giants near the galactic poles and found a chemical gradient of  $-0.4$  dex/kpc for the thin disk and a gradient of  $-0.18$  dex/kpc extending to  $z = 8$  kpc, a value that is identical with the one found in this study for  $z < 15$  kpc. Yoshii et al. (1987) derived a metallicity gradient of  $-0.5 \pm 0.1$  dex/kpc for  $z \leq 2$  kpc in logarithmic from UBV star count data by assuming the solar abundance in the Galactic plane, while this value is slightly steeper than the value of  $-0.37$  dex/kpc for  $z < 4$  kpc in this study. Jönch-Sörensen (1994) observed a sample of faint F-dwarfs in order to investigate the spatial distribution of metallicity in the disk of the Galaxy. They found a vertical gradient of  $-0.33$  dex/kpc for  $z \leq 500$  pc and  $-0.19$  dex/kpc for  $500 \leq z \leq 1500$  pc. Trefzger et al. (1995) found a rather steep mean metallicity gradient of  $-0.55 \pm 0.1$  dex/kpc up to  $z = 900$  pc and determined an overall gradient of  $-0.23$  dex/kpc for  $z < 4$  kpc, this gradient is slightly flatter than the one found in this study. We noted that these results are in close agreement, both quantitatively and qualitatively, with our finding at the high latitude fields. In Sect. 6, our results are similarly interpreted as a mixture of stellar population with different mean metallicities at all  $z$  levels.

## 6. THE METALLICITY GRADIENT ARISING FROM THE POPULATION GRADIENT

A crucial aid to the interpretation of these metallicity gradients is the varying contributions from the different Galactic components. As shown in Fig. 6, the expected relative number of stars from different components of the Galaxy is a function of height from the Galactic plane. The components are the thin disk, thick disk and halo. The thin disk population contains a young (age  $\leq 3$  Gyr), metal-rich population (mean abundance  $\langle[\text{Fe}/\text{H}]\rangle \sim 0.0$ ;  $\sigma_{[\text{Fe}/\text{H}]} \sim 0.15$ ), and a older (age  $\geq 3$  Gyr) more metal-poor population (mean abundance  $\langle[\text{Fe}/\text{H}]\rangle \sim -0.3$ ;  $\sigma_{[\text{Fe}/\text{H}]} \sim 0.2$ ) (Gilmore & Wyse 1985). The younger population contains  $\sim 20\%$  of the stars near the sun and has a vertical scale height  $\sim 100$  pc. The older population contains  $\sim 80\%$  of the stars near the sun, and is characterized by a exponential scale height of  $\sim 300$  pc. The young thin disk stars contribute up to  $z$  heights of around 300 pc and these old thin disk stars dominate from 300 pc to 1 kpc. Here, we only consider the old thin disk population in our model since we have very few samples of very nearby stars.

For the thick disk, Hartkopf & Yoss (1982) derived the mean abundance  $\langle[\text{Fe}/\text{H}]\rangle \sim -0.6$  and  $\sigma_{[\text{Fe}/\text{H}]} \sim 0.3$  with distances between 1 and 2 kpc; Buser (1999) also derived the mean metallicity of the thick disk  $\langle[\text{Fe}/\text{H}]\rangle \sim -0.63$  and dispersion  $\sigma_{[\text{Fe}/\text{H}]} \sim 0.4$  dex. Chiba & Beers (2000) showed that the thick disk population includes stars with a wide range of metallicity, from  $-2.2 \leq [\text{Fe}/\text{H}] \leq -0.5$ , and most of stars are in the more-rich end of this range. Recently, based on medium-resolution spectroscopy and broadband photometry, Beers et al. (2002) found that the local fraction of metal-poor stars which might be associated with the metal-weak thick disk is on the order of 30% – 40% at abundances below  $[\text{Fe}/\text{H}] = -1.0$ .



At the same time, they also found that this relatively high fraction of local metal-poor stars may extend to metallicities below  $[\text{Fe}/\text{H}] = -1.6$ , much lower than what had been considered before. For the halo, the field stars have similar mean metallicity with globular clusters in the Milky Way. However, the halo field stars extend to much lower metallicity ( $[\text{Fe}/\text{H}] \simeq -5$ ) than that of the globular clusters ( $[\text{Fe}/\text{H}] \simeq -2.2$ ) (Freeman et al. 2002). In general, it is adopted here that the halo mean abundance  $\langle [\text{Fe}/\text{H}] \rangle \sim -1.5$  and  $\sigma_{[\text{Fe}/\text{H}]} \sim 0.5$  (Gilmore & Wyse 1985).

In this study, we try to estimate the metallicity gradient resulting from changing relative proportions of different populations, assuming there doesn't exist a gradient for a single population. The number of stars at different heights  $z$  for three components (Fig. 6) could be combined with mean metallicity to produce estimates of metallicity distributions as a function of height above the plane. In order to check the mean metallicity's effect on the gradient, we divide the mean metallicities into two cases to discuss. In case A, the mean metallicities are  $\langle [\text{Fe}/\text{H}] \rangle \sim 0.0$  for the thin disk,  $\langle [\text{Fe}/\text{H}] \rangle \sim -0.6$  for the thick disk, and  $\langle [\text{Fe}/\text{H}] \rangle \sim -1.5$  for the halo, respectively. In case B, the mean metallicities are,  $\langle [\text{Fe}/\text{H}] \rangle \sim -0.3$  for the thin disk,  $\langle [\text{Fe}/\text{H}] \rangle \sim -1.0$  for the thick disk, and  $\langle [\text{Fe}/\text{H}] \rangle \sim -2.0$  for the halo, respectively. The mean parameter values in case A are in agreement with the majority of recent determinations, while the values in case B lie in the range of error of case A. The results are illustrated in Fig. 9; the dotted line and solid line represent case A and case B, respectively. The open circles represent the observational data. Many factors affect the determination of mean metallicity. The first source contributing to errors is from photometric errors; the second from stellar metallicity by fitting SEDs. In addition, there may exist an error from incompleteness of samples in each bin. As Fig. 9 shows clearly, although case B matches the observed metallicity distribution, both cases exhibit similar gradients for  $z < 5$  kpc and they become flat for  $z > 5$  kpc. Thus the gradient we derived ( $-0.37 \pm 0.1$  dex/kpc for  $z < 4$  kpc) can be interpreted as the different contributions in density distribution for the three components of the Galactic model, whereas the small or zero gradient  $d[\text{Fe}/\text{H}]/dz = -0.06 \pm 0.09$  can not be interpreted due to the different contributions from three components. In particular the last datum point ( $z \sim 15$  kpc) can be attributed to the incompleteness of the sample at that large distance. So it is possible that there is a little or no gradient for  $z > 5$  kpc. It should be noted that the low mean metallicity in case B is presumably a consequence of the selection effects (such as the magnitude, color selection and distance selection, etc.) involved in the definition of the sample. But this is an unimportant effect for the derivation of the gradient.

## 7. CONCLUSIONS AND SUMMARY

In this work, based on the BATC multicolor photometric system, we develop a calibration of temperature and metallicity for the dwarfs by employing a set of synthetic flux spectra calculated from theoretical models. Some temperature-sensitive color indices in the BATC filter system are found to

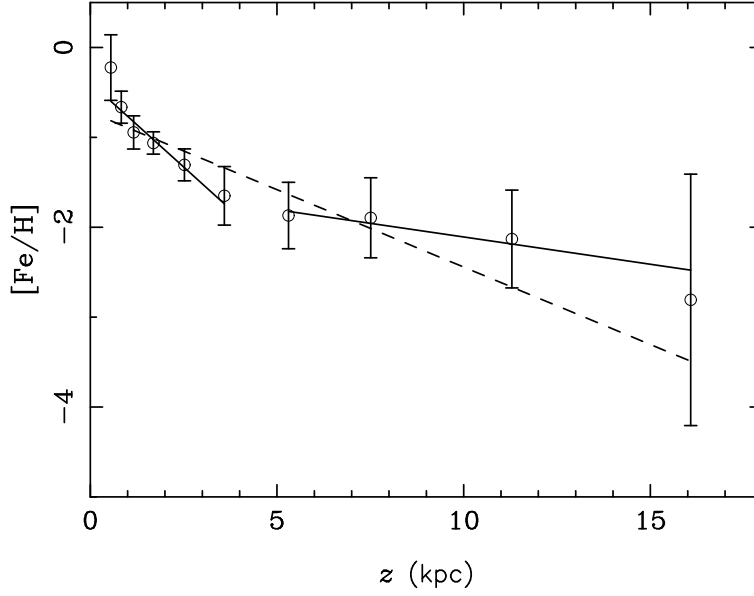


Fig. 8.— Mean metallicity distribution versus mean  $z$ -distance (kpc) for 10  $z$ -intervals, showing a metallicity gradient  $d[\text{Fe}/\text{H}]/dz \sim -0.37$  dex/kpc for  $z < 4$  kpc and  $d[\text{Fe}/\text{H}]/dz \sim -0.06$  dex/kpc (or possibly zero) between 5 and 15 kpc

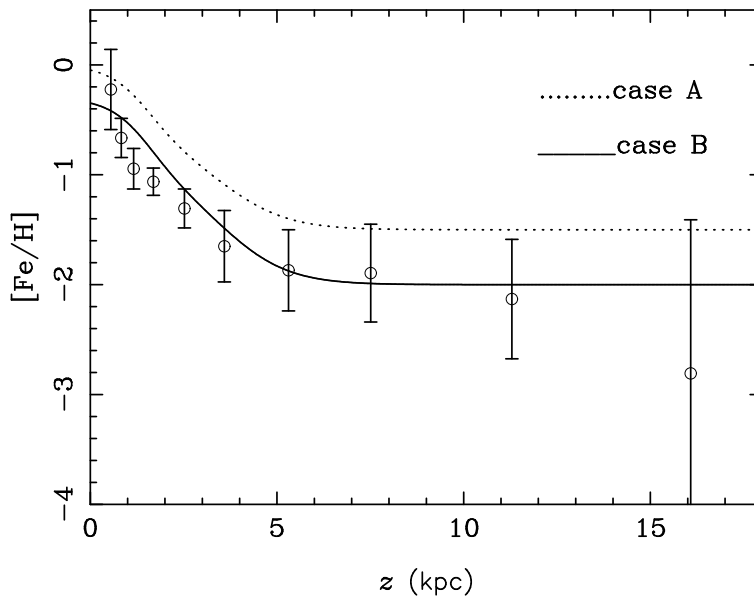


Fig. 9.— Observed and calculated mean metallicity distribution as a function of height  $z$ . The results of case A (dotted line) and case B (solid line) are illustrated.

yield well-defined linear relations with  $\log(T_{\text{eff}})$  (see Fig. 3). **More importantly, this study shows that in using the BATC multicolor observations not only can we conveniently assess stellar temperature, but metallicity and gravity as well.** We thus have confirmed the fact that stars can be successfully classified three-dimensionally from the BATC SEDs.

In addition, in this paper, by using F/G dwarfs of two BATC fields, we determined the average stellar metallicity as a function of distance from the galactic plane. It can clearly be seen that the mean metallicity decreases with increasing  $z$ , namely, we find a gradient of  $-0.37 \pm 0.1$  dex/kpc for  $z < 4$  kpc, whereas it shows a weak gradient between 5 and 15 kpc, i.e.,  $d[\text{Fe}/\text{H}]/dz = -0.06 \pm 0.09$  dex/kpc. The overall distribution shows a metallicity gradient  $d[\text{Fe}/\text{H}]/dz = -0.17 \pm 0.04$  dex/kpc, up to 15 kpc. These results are in agreement with the values in the literature (Yoshii et al. 1987; Yoss et al. 1987; Trefzger et al. 1995). In our study, these results are interpreted as different contributions from three components of the Galaxy at different  $z$  distances. In star counts the younger metal-rich stars are confined to regions close to the Galactic mid-plane, while the older, metal-poorer stars with a larger scale height dominate at larger vertical distances from the Galactic plane. As a consequence, a vertical metallicity gradient is caused by the varying dominance of different stellar components of the Galaxy. It is possible that additional observational investigations will give more evidence for the metallicity gradient of the Galaxy and therefore provide a powerful clue to the disk and halo formation because it almost certainly concerns events during and shortly after the early Galactic collapse and the beginning of disk formation (Sandage 1981; Bell 1996; Norris & Ryan 1991).

We would like to thank the referee, Dr. Yoss, for his insightful comments and suggestions that improved this paper greatly. The BATC Survey is supported by the Chinese Academy of Sciences, the Chinese National Natural Science Foundation under the contract No. 10273012 and the Chinese State Committee of Sciences and Technology. This work has been supported by the National Key Basic Research Science Foundation (NKBRSF TG199075402). We also thank the assistants who helped with the observations for their hard work and kind cooperation.

## REFERENCES

- Ardeberg, A., Lindgren, H. Nissen, P. E., 1983, A&A, 128, 194
- Beers, T. C., Flynn, K., Gebhardt, K., 1990, AJ, 100, 32
- Beers, T. C., Derilling, J.S., Rossi, S., et al., 2002, AJ, 124, 931
- Bell, D. J., 1996, AJ, 108, 1139
- Buser, R., Rong, J. X., 1995b, in Unresolved Problems of the Milky Way, IAU Symp. 169, ed. L.Biltz, Dordrecht: Kluwer
- Buser, R., Rong, J. X., Karaali, S., 1999, A&A, 348, 98
- Carraro, G., Ng, Y. K., Portinari, L., 1998, MNRAS, 296, 1045
- Cameron, L. M., 1985, A&A, 147, 47
- Chen, A. B., Tsay, W., Tsai, W., Lu, P. K., 2000, AJ, 120, 2569
- Chen, B., Stoughton, C., Smith, J. A., 2001, ApJ, 553, 184
- Chen, L., Hou, J. L., Wang, J. J., 2003, AJ, 125, 1397
- Chen, Y. Q., Nissen, P. E., Zhao, G., et al., 2000, A&AS, 141, 491
- Chiba M., Beers T., 2000, AJ, 119, 2843
- Crawford, D. L., 1975a, AJ, 80, 955
- Du, C. H., Zhou, X., Ma, J., et al., 2003, A&A, 407, 541
- Fan, X. H., Burstein, D., Chen, J. S., et al. 1996, AJ, 112, 628
- Fenkart, R., Esin-Yilmaz, F., 1985, A&AS, 62, 39
- Freeman, K., Bland-Hawthorn, J., 2002, ARA&A, 40, 487
- Friel, E. D., 1988, AJ, 95, 1727
- Friel, E. D., 1995, ARA&A, 33, 381
- Gilmore, G., Reid, N., 1983, MNRAS, 202, 1025
- Gilmore, G., Wyse, R. F. G., 1985, AJ, 90, 2015

- Gilmore, G., Wyse, R. F. G., Kuijken, K., 1989, *ARA&A*, 27, 555
- Grenon, M., 1977, in: Müller, E.A., (ed.) *Highlights of Astronomy*, Vol. 4, Part II. Reidel, Dordrecht
- Hartkopf, W. I., Yoss, K. M., 1982, *AJ*, 87, 1679
- Henry, R. B. C., & Worthey, G., 1999, *PASP*, 111, 919
- Hou, J. L., Prantzos, N., Boissier, S., 2000, *A&A*, 362, 921
- Jenkner, H., Lasker, B. M., Sturch, C. R., et al. 1990, *AJ*, 99, 2082
- Jönch-Sörensen H., 1994, Ph.D. Thesis, Copenhagen University
- Karaali, S., AK, S.G., Bilir, S., 2003, *MNRAS*, 343, 1013
- Kroupa, P., Tout, C. A., Gilmore, G., 1993, *MNRAS*, 262, 545
- Lejeune, T., Cuisinier, F., Buser, R., 1997, *A&AS*, 125, 229
- Maciel, W. J., Costa, R. D. D., Uchida, M. M. M., 2003, *A&A*, 397, 667
- Majewski, S. R., 1992, *ApJS*, 78, 87
- Majewski, S. R., 1993, *ARA&A*, 31, 575
- Neese, C. L., Yoss, K. M., 1988, *AJ*, 95, 463
- Nissen, P. E., 1981, *A&A*, 97, 145
- Norris, J., Green, E. M., 1989, *ApJ*, 337, 272
- Norris, J., Ryan, S. G., 1991, *ApJ*, 380, 403
- Ojha, D. K., Bienaymé, O., Robin, A. C., Crézé, M., 1996, *A&A*, 311, 456
- Oke, J. B., Gunn, J. E., 1983, *ApJ*, 266, 713
- Olsen, E. H., 1988, *A&A*, 189, 173
- Pasquali, A., & Perinotto, M., 1993, *A&A*, 280, 581
- Piatti, A. E., Claria, J. J., Abadi, M. G., 1995, *AJ*, 110, 281
- Pickles, A. J., 1998, *PASP*, 110, 863
- Ratnatunga, K. U., Freeman, K. C., 1989, *ApJ*, 339, 126

- Reid, N. I., Majewski, S. R., 1993, ApJ, 409, 635
- Robin, A. C., Haywood, M., Crézé, M., 1996, A&A, 305, 125
- Sandage, A., 1981, AJ, 86, 1643
- Sandage, A., Fouts, G., 1987, AJ, 93, 74
- Sandage, A., 1990a, J.R. Astron. Soc. Can., 84, 70
- Schuster, W. J., Nissen, P. E., 1989, A&A, 221, 65
- Shaver, P. A., McGee, R. X., Newton, L. M., et al. 1983, MNRAS, 204, 53
- Stetson, P. B., 1987, PASP, 99, 191
- Trefzger, C. H., Pel, J. W., Gabi, S., 1995, A&A, 304, 381
- Wallerstein, G., 1962, A&AS, 6, 407
- Xia, L. F., Zhou, X., Ma, J., et al. 2002, PASP, 114,1349
- Yamagata T., Yoshii, Y., 1992, AJ, 103, 117
- Yoss, K. M., Hartkopf, W. I., 1979, AJ, 84, 1293
- Yoss, K. M., Neese, C. L., Hartkopf, W. I., 1987, AJ, 94, 1600
- Yoshii, Y., Ishida, K., Stobie, R. S., 1987, AJ, 93, 323
- Zhou, X., Jiang, Z. J., Xue, S. J., et al. 2001, ChJAA, 1, 372
- Zhou, X., Jiang, Z. J., Ma, J., et al. 2003, A&A, 397, 361